Structural rearrangements and reaction intermediates in a di-Mn water oxidation catalyst

Valles-Pardo, J.L.; Groot, H.J.M. de; Buda, F.

PCCP

Cite this: *Phys. Chem. Chem. Phys.*, 2012, **14**, 15502–15508

www.rsc.org/pccp

PAPER

Structural rearrangements and reaction intermediates in a di-Mn water oxidation catalyst

J. L. Vallés-Pardo, H. J. M. de Groot and F. Buda*

Received 19th July 2012, Accepted 28th September 2012
DOI: 10.1039/c2cp42466e

By using first-principles molecular dynamics simulations combined with metadynamics to simulate rare events we analyse competing reaction coordinates for a di-Mn water oxidation catalyst ([(bis(imino)pyridine)(H_2O)Mn^{IV}(μ-O)$_2$$Mn^{V}$(O)(bis(imino)pyridine)]$^{3+}$). The catalytic water oxidation cycle of the complex is examined by addressing the thermodynamic accessibility of the hydroperoxo species that is considered a critical and rate-limiting intermediate. To achieve this, hybrid quantum-mechanics/molecular-mechanics (QM/MM) and full QM simulations have been performed for an explicit treatment of the water environment that plays an active role in the reaction processes. Starting from a likely active species for the O–O bond formation, we observe that during the water approach to the oxo ligand a facile structural rearrangement of the complex takes place, leading to the opening of one μ-O bridge and the release of a water ligand, and resulting in two pentacoordinated Mn centers. This complex appears weakly active in the water oxidation process, since a concerted reaction is required to establish a Mn–OOH hydroperoxo intermediate. The slow kinetics of a concerted reaction can allow other processes, including linear degradation of the catalyst, to take precedence over catalytic water oxidation.

1. Introduction

A key process in natural photosynthesis is the four-electron four-proton water oxidation reaction producing O_2. This reaction takes place in the oxygen evolving complex (OEC) of photosystem II (PSII), which consists of a tetramanganese cluster with several oxo-bridges.[1] A mechanistic insight in the water splitting process is fundamental for the development of artificial devices for solar energy storage. High resolution crystallographic, EXAFS and spectroscopic data, combined with computational modeling, mostly based on Density Functional Theory (DFT), have recently provided structural and mechanistic insight in the catalytic cycle taking the OEC through the states S_0 to S_4.[2–6] In parallel there has been a growing effort in synthesizing biomimetic complexes that could efficiently perform the catalytic O_2 formation from water.[7] An optimal catalyst for water oxidation should properly address various requirements, most noticeably a good efficiency, low cost, and good stability. Man made catalysts are mostly based on Ru, and Co,[8–12] and the search for complexes based on more abundant elements, such as Mn or Fe, is progressing.[13,14] One of the first successful attempts in this direction is the Mn-complex [H_2O(terpy)Mn(O)$_2$Mn-(terpy)OH_2]$^{3+}$ (terpy = 2,2′:6,2″-terpyridine), which contains two Mn atoms linked by two μ-oxo bridges.[15] This complex is able to catalyze the formation of O_2 from water, although it also shows a high degree of deactivation by ligand loss and permanganate formation.[16–19]

Since the catalyst is based on Mn and uses more than one metal ion connected by oxo-bridges, in a way similar to the natural OEC, this catalyst has been the subject of extensive theoretical investigations to elucidate the nature of the key intermediates in the catalytic cycle.[13,20,21] On the basis of density functional theory (DFT) calculations, it has been suggested that the active species in the O–O bond formation step is the [(bis(imino)pyridine)(H_2O)Mn^{IV}(μ-O)$_2$$Mn^{V}$(O)-(bis(imino)pyridine)]$^{3+}$ complex (**1**).[20] In a recent work by Nakamura *et al.*, an alternative reaction path for oxygen formation has been proposed based on a direct involvement of excess oxidants acting as counterions, such as OCl^-.[22] Most of the previous theoretical mechanistic studies address hypothetical transition states and intermediates in a static approach and do not include an explicit description of the water solvation.

In this study we use *ab initio* molecular dynamics simulations with an additional time-dependent bias potential along specific reaction coordinates as proposed by Laio and Parrinello.[23] Both hybrid quantum-mechanics/molecular mechanics (QM/MM) and full QM simulations are employed to include explicitly the solvent environment. In this way we can explore several potential reaction paths including dynamics and solvation effects. We consider here mechanisms in which the oxygen atoms originate from water and not from an oxygen-based oxidant. The simulations show that

Leiden Institute of Chemistry, Leiden University, P.O. Box 9502, 2300 RA Leiden, The Netherlands.
E-mail: f.buda@chem.leidenuniv.nl; Fax: +31 (0)71 5274603; Tel: +31 (0)71 5275723

the di-Mn cluster can undergo a structural rearrangement and form a complex that is weakly active in the O–O bond formation. The slow kinetics of this step can allow other processes, including linear degradation of the catalyst, in line with the deactivation processes observed experimentally.[16–19] These results can help to guide the chemical design of molecular scaffolds with specific structural features for the implementation of stable water oxidation catalysts with improved durability.

2. Computational details

The *ab initio* molecular dynamics (AIMD) simulations in this work were performed with the CPMD program.[24] Nuclear forces in AIMD are derived from the electronic structure using DFT with the BLYP functional.[25,26] The choice of a non-hybrid functional is mostly dictated by computational efficiency in the AIMD. However, single point calculations using the hybrid functionals OPBE0, B3LYP, B3LYP*,[27] that differ in the amount of exact exchange (25%, 20% and 15%, respectively), have been performed with the ADF program[28–30] to check the relative energy of different complexes in order to validate the BLYP results. Further tests have been performed with the ADF program to check the effect of empirical dispersion corrections in the form proposed by Grimme.[31]

We use norm-conserving pseudopotentials of the Martins–Troullier[32] form for all the atomic elements except for Mn, for which we used the Godecker form.[33] The Kohn–Sham orbitals are expanded on a plane-waves basis set with an energy cutoff of 100 Ry, which provides a good convergence in relative energies.

For the Car-Parrinello AIMD simulations we took a time step $\Delta t = 5$ a.u. and a fictitious electronic mass $\mu = 400$ a.u. In order to efficiently explore possible reaction pathways, we use the CPMD code with the metadynamics approach.[23] The metadynamics is a coarse-grained dynamics on the free-energy surface (FES) defined by a few collective variables, such as distances, angles, and coordination numbers. The method uses an adaptive bias potential to escape from local minima. In our simulations we evolve the collective variables with one metadynamics step every ten AIMD time steps. At each metadynamics step the evolution of the collective variables is guided by a generalized force that combines the action of the thermodynamic force, which would trap the system in a free energy minimum, and a history-dependent force that disfavors configurations already visited. This history-dependent potential is built as a sum of Gaussian functions centered in the explored values of the collective variables. The width and height of the Gaussian are parameters that can be tuned to find the best compromise between accuracy in the FES estimate and speed in crossing energy barriers to sample the whole collective variable space. Generally we used default values of 0.1 a.u. and 0.001 Hartree, respectively. In this work metadynamics simulations are used to explore hypothetical reaction paths rather than to accurately estimate free-energy barriers.

For a more realistic study of the reaction we include explicitly the solvent environment within a QM/MM approach as implemented in the CPMD code.[34] QM/MM simulations are performed in a cubic box of 33 $Å^3$ containing our di-Mn catalyst and about 1000 water molecules. The di-Mn cluster and a few (3–4) closest water molecules that can play an active role in the reaction are included in the QM subsystem treated at the DFT level, while the remaining water molecules are treated with Molecular Mechanics (MM). For the MM part the AMBER force field is used with the TIP3P model for the water molecules.[35] The solvent environment is equilibrated at room temperature with a classical MD while the Mn complex is kept fixed. In addition, we perform AIMD simulations for complex **2** with a full QM water environment, in which we include 72 water molecules in a box 20.5 × 23.8 × 18.1 Å.

3. Results and discussion

3.1 Modeling of the Hexa-coordinated complex with two oxo-bridges (1)

3.1.1 Structural and electronic characterization. In order to validate the choice of the functional and basis set described in the previous section, we compare the structural and electronic properties of complex **1** with DFT results that were obtained for the same model using a hybrid functional.[20] We optimize the geometry of complex **1** for different multiplicities and report the resulting relevant geometrical parameters and relative energies in Table 1 (see also Fig. 1 for the atomic labelling). First we notice that the most stable spin state and the order of higher energy multiplicities are consistent with previous DFT results.[20] In particular, the energy difference between the lowest energy doublet and the sextet is found to be 5.6 kcal mol^{-1} in BLYP *vs.* 3.04 kcal mol^{-1} in B3LYP. This difference is consistent with the general finding that a non-hybrid functional, like the BLYP, favours the low spin states over the high spin states, contrary to hybrid functionals. In Table 1 we also report the bond lengths obtained in ref. 20 for the lowest energy (doublet) spin state.

Overall the bond lengths obtained with BLYP are similar to those obtained with B3LYP, the larger difference being found for d(Mn2–O3) which is 0.15 Å shorter in our calculation. As already discussed in ref. 20, a shorter Mn–oxo ligand distance corresponds with a weaker radical character of the oxygen,

Table 1 Relative energy and important bond lengths in the di-Mn cluster **1**

Multiplicity	Relative energy	Mn2–O3	Mn1–O4	Mn1–O5	Mn2–O4	Mn2–O5
2	0	1.61	1.79	1.75	1.79	2.09
6	5.6	1.61	1.80	1.74	1.81	2.10
2	7.9	1.61	1.79	1.75	1.79	2.09
8	29.6	1.83	1.79	1.77	1.85	1.94
2[a]		1.76	1.80	1.73	1.83	1.96

[a] From ref. 20. Bond lengths are given in Å and relative energies in kcal mol^{-1}. For the atomic labeling we refer to Fig. 1.

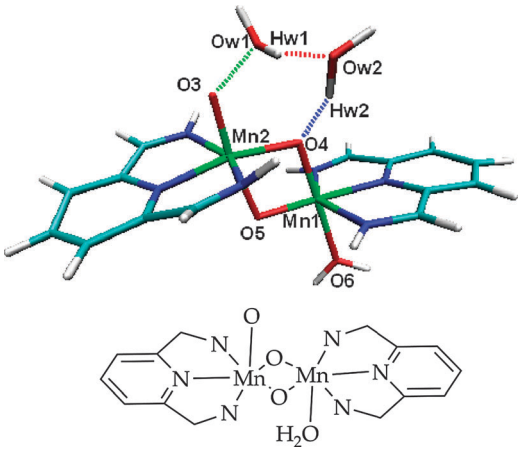

Fig. 1 Di-manganese complex **1** with two water molecules. The dashed lines represent the collective variables used in the metadynamics simulation. The atomic labeling used throughout the paper is indicated.[40] For clarity we also show a schematic drawing of the complex in the bottom.

which is also confirmed by the analysis of the spin density. It has been observed that the spin population on the Mn and on the oxo ligand can be tuned by varying the contribution of exact exchange in the functional and it is difficult to assess without a direct comparison with experiment which functional gives the most accurate description of the spin localization in the complex.[36] Additional calculations performed with the ADF program, a TZP basis set, and including dispersion corrections in different functionals give Mn–O distances close to 1.60 Å both with BLYP than with hybrid functionals (see Table 2). As mentioned above this distance is usually associated more with a Mn–oxo rather than a Mn–oxyl radical. However, the Mulliken spin population analysis does not provide an unambiguous picture for the O ligand in complex **1** since no clear trend emerges in going from standard GGA to hybrid functionals, with the BLYP-D and B3LYP*-D functionals giving −0.20 and 0.03 respectively, and OPBE0-D predicting a stronger radical character (0.67).

Table 2 Manganese–oxygen distances in the di-Mn complexes **1–3**

Complex **1**		
Functional	Mn2-O3	Mn1-O6
BLYP	1.62	2.16
BLYP-D	1.62	2.13
B3LYP*-D	1.60	2.10
OPBE0-D	1.54	2.11
Complex **2**		
Functional	Mn1–Ox1	Mn2–Ox2
BLYP	1.60	1.62
BLYP-D	1.60	1.62
B3LYP*-D	1.57	1.57
OPBE0-D	1.55	1.53
Complex **3**		
Functional	Mn–OOH	Mn–OH
BLYP	1.82	1.84
BLYP-D	1.81	1.83
B3LYP*-D	1.73	1.77

Bond lengths are given in Å. For the atomic labeling we refer to Fig. 1 and 4.

3.1.2 Reaction pathway analysis for complex 1. We first explore the reaction pathway involving the oxygen bond formation between one water molecule and the oxyl radical and the concerted jump of one water hydrogen to the oxo bridge, following the suggestion based on early DFT calculations.[20] A geometry optimization of complex **1**, including a water molecule initially located between the oxyl radical and one oxo-bridge, leads to a stable conformation where the water forms hydrogen bonds with both aromatic ligands. Starting from this optimized geometry, we perform a metadynamics simulation with two collective variables: The distance between the water oxygen and the oxyl radical, and the distance between one water hydrogen and one oxo-bridge, assuming that the oxo bridge can act as a proton acceptor in this reaction step. The maximum value for the collective variables was set to 3 Å. During this metadynamics we can observe the water hydrogen (Hw) approaching the oxo-bridge (up to ∼1 Å distance). However, when the hydrogen reaches this configuration, the oxyl radical–water oxygen (Ox–Ow) distance is not short enough for a reaction to occur.

In a genuine solvent environment, other water molecules in the coordination sphere of the catalyst can facilitate the proton transfer step. Therefore we added a second water molecule in a position where it can act as a proton channel from the first water to the oxo-bridge. To test if a reaction pathway is possible where the Ox–Ow bond formation is accompanied by a proton jump through the second water onto the oxo-bridge, we include a bias potential for each of the bonds that we expect to be formed during this reaction (see Fig. 1). Along this trajectory, we observe a structural rearrangement of complex **1**, as illustrated in Fig. 2:

The aquo ligand breaks its coordination bond and at the same time one of the oxo-bridges opens up and the oxygen moves into the initial position of the aquo ligand. As a consequence of this internal rearrangement, the two manganese atoms become pentacoordinated. To verify that this structural rearrangement is not an artifact of the lack of a proper environment, we repeated this metadynamics simulation in water within the QM/MM approach (see Computational Details section). In this case however, we consider only the Ox–Ow distance as a collective variable and allow all the other degrees of freedom to evolve freely. In this way we do not force the proton to jump onto the oxo-bridge, which might

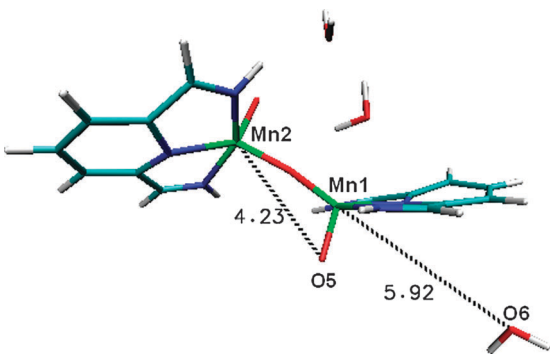

Fig. 2 Snapshot of the di-manganese complex after 1700 MD steps. The Mn2–O5 and Mn1–O6 distances (Å) are shown to underline the structural changes observed in the simulation.[40]

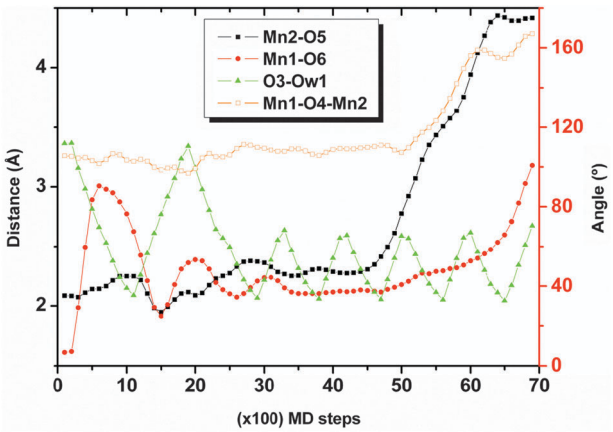

Fig. 3 Relevant geometrical parameters during the structural rearrangement of complex **1** observed in the QM/MM simulation including the water environment.

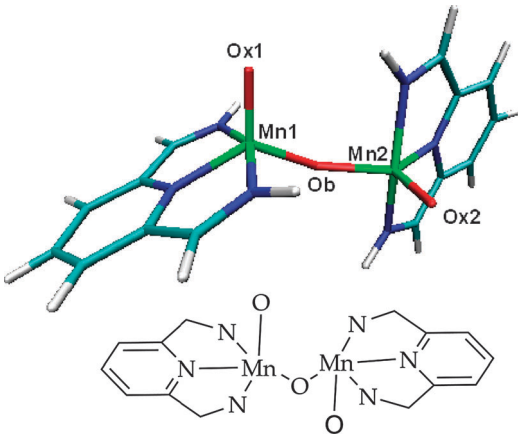

Fig. 4 Optimized geometry of complex **2**.[40] For clarity we also show a schematic drawing of the complex in the bottom.

induce the structural instability. The results are shown in Fig. 3, where a similar structural rearrangement as observed in vacuum takes place. The opening of the oxo-bridge (orange and black lines) and the leaving of the aquo ligand (red line) occur prior to any attempt of bond formation between the oxo ligand and the oxygen water (green line), or in other words before the water oxidation process could take place. Indeed the minimum O3–Ow1 distance is ~2 Å, in spite of the bias potential, suggesting that an activation barrier associated with the transition state is encountered at this distance.

It should be mentioned that a spin crossing might occur during a reaction involving bond splitting as discussed in ref. 10 and 37. Here however the structural rearrangement occurs before any sign of water splitting and therefore we have not considered a different spin state in the metadynamics simulations.

In the simulations, the structural rearrangement has lower activation energy than the oxygen–oxygen bond formation. In addition, our findings underline that the oxo-bridge is not a proper proton acceptor for this catalytic reaction step. This is well in line with a theoretical study on a similar di-Ru catalyst, indicating that the hydrogen jump to the μ-oxo moiety requires a substantial structural distortion and is not thermodynamically stable.[38]

3.2 Modeling of the penta-coordinated manganese cluster (2) with one oxo-bridge

3.2.1 Structural and electronic characterization of complex 2. A geometry optimization is performed to check the structural stability of the penta-coordinated di-Mn complex [(bis(imino)pyridine)-(O)Mn^{IV}(μ-O)Mn^{V}(O)(bis(imino)pyridine)]$^{3+}$ (**2**) obtained after the structural rearrangement of complex **1**. Also for complex **2** we find that the doublet state is the lowest energy as for complex **1**. This conclusion is true both in vacuum and in explicit water environment with the quartet state being about 6 kcal mol^{-1} higher in energy. The spin density shows antiferromagnetically coupled manganese centers similarly to complex **1**. A Mulliken spin population analysis at the BLYP level gives 1.20 for Mn1 and −0.39 for Mn2. In addition, one oxo ligand shows a higher spin population (Ox1, 0.27) than the other one (Ox2, −0.10). In Table 2 it can be noticed that the Mn–O distances obtained with different functionals for complex **2** are very similar to those obtained for complex 1. The optimized geometry (see Fig. 4) shows a dihedral angle (θ) Ox1–Mn1–Mn2–Ox2 of ~90°, which could facilitate a hypothetical water oxidation path where one of the two oxo ligands can act as proton acceptor.[38]

To assess whether the structural rearrangement of complex **1** is thermodynamically accessible, we show in Table 3 the energy difference between complex **1** and complex **2** plus one water molecule [$\Delta E = E(\mathbf{2} + \text{water}) - E(\mathbf{1})$] for various functionals and basis sets, including hybrid functionals and dispersion corrections.

The energy comparison shows that the one oxo-bridge complex **2** is thermodynamically more stable than the two oxo-bridges complex **1** although the energy difference varies considerably from one functional to the other with the BLYP functional giving the smallest energy difference.

3.2.2 Reaction pathway analysis for complex 2. Having established that the complex **2** is stable and thermodynamically favorable, we explore now its potential water oxidation activity. A likely hypothetical reaction pathway involves the approach of the oxygen of a water molecule to one oxo ligand and a proton jump from the water molecule to the other oxo ligand.

We first consider complex **2** plus a water molecule located between the two oxo ligands as a starting configuration for metadynamics investigations in vacuum. During the simulation with only the Ox1–Ow distance as collective variable we observe

Table 3 Energy difference between complex **1** and complex **2** plus one water molecule [$\Delta E = E(\mathbf{2} + \text{water}) - E(\mathbf{1})$], optimized using different functionals and basis sets. STO (TZP) is a triple zeta with polarization Slater type basis set and PW (100 Ry) is a plane wave basis set with a cutoff of 100 Ry. We show also the effect of empirical dispersion corrections (D) included using the Grimme parameters[31]

Basis set	Functional	ΔE (kcal mol^{-1})
PW (100 Ry)	OPBE	−28.9
STO (TZP)	BLYP	−6.5
STO (TZP)	BLYP-D	−1.9
STO (TZP)	B3LYP	−15.1
STO (TZP)	B3LYP*-D	−13.9
STO (TZP)	OPBE0-D	−25.7

that as soon as the water oxygen approaches one oxo ligand (dOx1–Ow ~ 1.6 Å) the Mn1–Ox1 distance starts to increase considerably, indicating a weakening of the manganese-oxygen bond. However, the hydrogen of the water is not transferred to the other oxo ligand, and remains at a distance longer than 3 Å. By adding a bias potential along the distance between a hydrogen of the approaching water and the other oxo ligand, while at the same time keeping the Ox1–Ow distance close to the bonding value, we can observe a rapid proton transfer from the water to the other oxo ligand, leading to the expected product (see Fig. 5). This result suggests that the proton jump occurs easily when the oxygen–oxygen bond is already formed. By comparing the energy of complex **2** plus a water against the resulting [(bis(imino)pyridine)(OOH)Mn^{IV}(μ-O)Mn^{V}(OH)-(bis(imino)pyridine)]$^{3+}$ intermediate complex (**3**), we can conclude that this step is endothermic. In Table 4 the results obtained with different functionals are shown. We can observe that hybrid functionals predict a smaller energy difference and a spin crossing from a doublet to a quartet spin state.

In order to check whether the solvent environment can facilitate this reaction step by playing the role of proton acceptor,[10] we perform AIMD simulations with a full QM description of the water environment (see Computational Details section). The solvate environment provides a hydrogen bonding network between various water molecules, which can allow

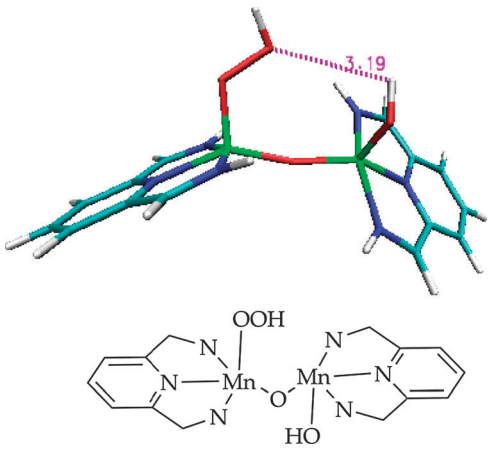

Fig. 5 di-Mn complex intermediate after formation of the O–O bond and proton jump to the second oxo ligand.[40] For clarity we also show a schematic drawing of the complex in the bottom.

Table 4 Energy difference between complex **2** plus one water molecule and complex **3** [$\Delta E = E(3) - E(2 + \text{water})$], optimized using different functionals. The first entry BLYP (PW) is the result obtained with the CPMD program using plane waves with 100 Ry cutoff. All other results are obtained with the ADF program and a triple zeta with polarization Slater type basis set (STO/TZP). The effect of empirical dispersion corrections (D)[31] is also shown. The results are presented for doublet to doublet and for a spin crossover from doublet to quartet

Functional	$\Delta E_{\text{doublet} \rightarrow \text{doublet}}$ (kcal mol^{-1})	$\Delta E_{\text{doublet} \rightarrow \text{quartet}}$ (kcal mol^{-1})
BLYP (PW)	—	37.5
BLYP	24.0	33.7
BLYP-D	23.3	33.0
B3LYP-D	23.2	10.4
B3LYP*-D	21.4	12.8

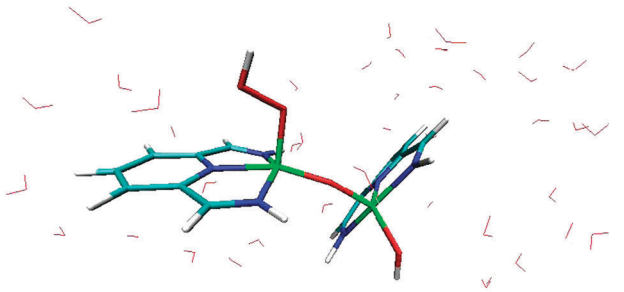

Fig. 6 Snapshot of the stable Mn–OOH intermediate (complex **3**) taken from a AIMD simulation in fully QM water environment at room temperature without any constraint.[40]

for the proton of the reactant water molecule to jump more easily to the other oxo ligand or be solvated in the environment. Initially we perform a metadynamics simulation with a bias potential acting on the Ox1–Ow distance between the oxo ligand and the closest water. When the Ox1–Ow distance is decreasing and approaching a typical O–O bond length value of ~ 1.4 Å, we observe as expected an increase in the Mn–Ox distance as well as an increase in the internal water Hw–Ow distance. However, a complete proton transfer to the other oxo ligand or to the water environment is never observed. This may be due to the fact that in the metadynamics simulations the evolution of the CV is quicker than the equilibration time needed by the solvent to reorganize to the current Ox1–Ow distance in order to facilitate the proton release.

For this reason we perform additional AIMD simulations without any constraint in which we start from the complex with the formed hydroperoxo ligand and with the released proton relocated in the water environment. In all cases we observe that the hydroperoxo ligand is not stable, the Ox1–Ow distance increases, leading to the breakage of the bond, and the released OH^- reconstitutes a water molecule with the proton present in the solvent.

However, starting the AIMD simulation with the formed hydroperoxo ligand and with the released proton on the other oxyl ligand (as in complex **3**), we can observe that the hydroperoxo ligand and the whole intermediate complex is stable in the water environment (Fig. 6).

From these simulations we can conclude that the oxygen–oxygen bond formation step occurs only if at the same time the second oxyl ligand accepts a proton, thereby keeping the total charge of the complex unchanged. Hence complex **2** appears to be weakly active towards the formation of the O–O bond since the formation of intermediate **3** requires a thermodynamically difficult concerted reaction step.

4. Conclusions

The search for a water oxidation catalyst based on abundant transition metals is currently an important step in the development of artificial photosynthesis devices. Specifically Mn catalysts with oxo-bridges mimicking the natural OEC of photosystem II are being explored as possible candidates for this goal. Here we focus on the reactivity of a di-Mn cluster that has been the subject of experimental and theoretical studies for more than a decade. Our results based on *ab initio*

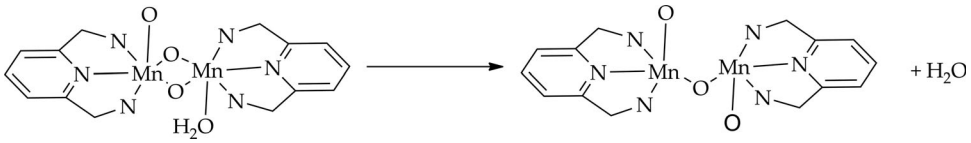

Scheme 1 Structural rearrangement of complex **1** to form complex **2** with a release of a water molecule in the solvent environment.

MD simulations at room temperature, including explicitly the solvent environment, clearly show that the cluster can easily undergo a structural rearrangement involving a breakage of one of the oxo-bridges and a release of a water ligand leading to two pentacoordinated Mn sites (see Scheme 1). These computational results are in line with previous experimental work on this di-Mn cluster,[15] in which it has been observed that the catalytic activity in aqueous solution decreases dramatically after a few cycles. It has been reported that permanganate ions or manganese oxide particles are usually the decomposition products of these Mn based catalysts. Moreover, the well known Ru based blue dimer catalyst also shows reductive cleavage of the bridging oxido ligand, similarly to our proposed structural rearrangement.[19] We suggest that when the two-oxo bridged cluster is in water, after a few catalytic cycles, the structural rearrangement takes place. This rearrangement leads to a complex (**2**) that is poorly active toward the O–O bond formation: Indeed the formation of the new oxygen–oxygen bond step requires a very specific hydrogen bonding network in order to perform a concerted proton jump to convert the second oxo ligand into an hydroxo ligand. This can explain the decrease in the activity shown in the experimental work.

It has been pointed out that in the natural OEC the flexibility of the Mn–O–Mn angles is a key feature in facilitating the water oxidation process.[5] However we observe that this structural flexibility in the bending of the two oxo-bridges can culminate in the opening of one of the bridges, thereby degrading the catalyst.[16–18] In the natural OEC the protein matrix in which the Mn complex is embedded provides extra stability to the catalyst, while allowing for some structural distortions to take place during the S_0–S_4 cycle. Thus we suggest that a proper design of the catalyst should include the design of a smart embedding matrix minimizing structural distortions leading to degradation of the catalyst, while providing the proper channels for water and proton dynamics. Anchoring the water oxidation catalyst to a nanoparticle[21] or to a oxide surface,[39] can already provide a more robust system in aqueous and oxidative conditions.

Acknowledgements

The use of supercomputer facilities was sponsored by NWO Physical Sciences, with financial support from the Netherlands Organization for Scientific Research (NWO). This research is financed in part by the BioSolar Cells open innovation consortium, supported by the Dutch Ministry of Economic Affairs, Agriculture and Innovation (project C1.9).

References

1 Y. Umena, K. Kawakami, J.-R. Shen and N. Kamiya, *Nature*, 2011, **473**, 55–60.
2 B. Kok, B. Forbush and M. McGloin, *Photochem. Photobiol.*, 1970, **11**, 457–475.
3 J. Yano, J. Kern, K. Sauer, M. J. Latimer, Y. Pushkar, J. Biesiadka, B. Loll, W. Saenger, J. Messinger, A. Zouni and V. K. Yachandra, *Science*, 2006, **314**, 821–825.
4 R. D. Britt, K. A. Campbell, J. M. Peloquin, M. L. Gilchrist, C. P. Aznar, M. M. Dicus, J. Robblee and J. Messinger, *Biochim. Biophys. Acta*, 2004, **1655**, 158–171.
5 P. E. M. Siegbahn, *Acc. Chem. Res.*, 2009, **42**, 1871–1880.
6 E. M. Sproviero, J. A. Gascón, J. P. McEvoy, G. W. Brudvig and V. S. Batista, *J. Am. Chem. Soc.*, 2008, **130**, 3428–3442.
7 K. S. Joya, J. L. Vallés-Pardo, Y. Faheem, T. Eisenmayer, B. Thomas, F. Buda and H. J. M. de Groot, *ChemPlusChem*, 2012, DOI: 10.1002/cplu.201200161.
8 Y. Xu, T. Åkermark, V. Gyollai, D. Zou, L. Eriksson, L. Duan, R. Zhang, B. Åkermark and L. Sun, *Inorg. Chem.*, 2009, **48**, 2717–2719.
9 D. J. Wasylenko, C. Ganesamoorthy, B. D. Koivisto, M. A. Henderson and C. P. Berlinguette, *Inorg. Chem.*, 2010, **49**, 2202–2209.
10 J. L. Vallés-Pardo, M. C. Guijt, M. Iannuzzi, K. S. Joya, H. J. M. de Groot and F. Buda, *ChemPhysChem*, 2012, **13**, 140–146.
11 M. W. Kanan and D. G. Nocera, *Science*, 2008, **321**, 1072–1075.
12 F. Jiao and H. Frei, *Angew. Chem., Int. Ed.*, 2009, **48**, 1841–1844.
13 T. Wang, G. W. Brudvig and V. S. Batista, *J. Chem. Theory Comput.*, 2010, **6**, 2395–2401.
14 M. Z. Ertem, L. Gagliardi and C. J. Cramer, *Chem. Sci.*, 2012, **3**, 1293–1299.
15 J. Limburg, J. S. Vrettos, L. M. Liable-Sands, A. L. Rheingold, R. H. Crabtree and G. W. Brudvig, *Science*, 1999, **283**, 1524–1527.
16 J. Limburg, J. S. Vrettos, H. Chen, J. C. de Paula, R. H. Crabtree and G. W. Brudvig, *J. Am. Chem. Soc.*, 2001, **123**, 423–430.
17 R. Tagore, H. Chen, H. Zhang, R. H. Crabtree and G. W. Brudvig, *Inorg. Chim. Acta*, 2007, **360**, 2983–2989.
18 R. Tagore, H. Chen, R. H. Crabtree and G. W. Brudvig, *J. Am. Chem. Soc.*, 2006, **128**, 9457–9465.
19 B. Limburg, E. Bouwman and S. Bonnet, *Coord. Chem. Rev.*, 2012, **256**, 1451–1467.
20 M. Lundberg, M. R. A. Blomberg and P. E. M. Siegbahn, *Inorg. Chem.*, 2004, **43**, 264–274.
21 G. Li, E. M. Sproviero, W. R. McNamara, R. C. Snoeberger, R. H. Crabtree, G. W. Brudvig and V. S. Batista, *J. Phys. Chem.. B*, 2010, **114**, 14214–14222.
22 M. Hatakeyama, H. Nakata, M. Wakabayashi, S. Yokojima and S. Nakamura, *J. Phys. Chem. A*, 2012, **116**, 7089–7097.
23 A. Laio and M. Parrinello, *Proc. Natl. Acad. Sci. U. S. A.*, 2002, **99**, 12562–12566.
24 CPMD, http://www.cpmd.org/, Copyright IBM Corp 1990–2011, Copyright MPI für Festkörperforschung Stuttgart 1997–2001.
25 A. D. Becke, *Phys. Rev. A: At., Mol., Opt. Phys.*, 1988, **38**, 3098–3100.
26 C. Lee, W. Yang and R. G. Parr, *Phys. Rev. B: Condens. Matter Mater. Phys.*, 1988, **37**, 785–789.
27 A. D. Becke, *J. Chem. Phys.*, 1993, **98**, 5648–5652.
28 G. te Velde, F. M. Bickelhaupt, E. J. Baerends, C. Fonseca Guerra, S. J. A. van Gisbergen, J. G. Snijders and T. Ziegler, *J. Comput. Chem.*, 2001, **22**, 931–967.
29 C. Fonseca Guerra, J. G. Snijders, G. te Velde and E. J. Baerends, *Theoretical Chemistry Accounts: Theory, Computation, and Modeling (Theoretica Chimica Acta)*, 1998, **99**, 391–403.
30 *ADF, ADF2007.01, SCM, Theoretical Chemistry*, Vrije Universiteit, Amsterdam, The Netherlands, <http://www.scm.com/>.
31 S. Grimme, *J. Comput. Chem.*, 2006, **27**, 1787–1799.
32 G. J. Martyna and M. E. Tuckerman, *J. Chem. Phys.*, 1999, **110**, 2810–2821.
33 S. Goedecker, M. Teter and J. Hutter, *Phys. Rev. B: Condens. Matter Mater. Phys.*, 1996, 54.

34 M. Eichinger, P. Tavan, J. Hutter and M. Parrinello, *J. Chem. Phys.*, 1999, **110**, 10452.
35 AMBER, D. A. Case, T. A. Darden, T. E. Cheatham III, C. L. Simmerling, J. Wang, R. E. Duke, R. Luo, R. C. Walker, W. Zhang, K. M. Merz, B. Roberts, S. Hayik, A. Roitberg, G. Seabra, J. Swails, A. W. Goetz, I. Kolossvai, K. F. Wong, F. Paesani, J. Vanicek, R. M. Wolf, J. Liu, X. Wu, S. R. Brozell, T. Steinbrecher, H. Gohlke, Q. Cai, X. Ye, J. Wang, M.-J. Hsieh, G. Cui, D. R. Roe, D. H. Mathews, M. G. Seetin, R. Salomon-Ferrer, C. Sagui, V. Babin, T. Luchko, S. Gusarov, A. Kovalenko and P. A. Kollman, *AMBER 12*, University of California, San Francisco, 2012.
36 C. Herrmann, M. Podewitz and M. Reiher, *Int. J. Quantum Chem.*, 2009, **109**, 2430–2446.
37 L. Bernasconi, P. Belanzoni and E. J. Baerends, *Phys. Chem. Chem. Phys.*, 2011, **13**, 15272–15282.
38 X. Yang and M.-H. Baik, *J. Am. Chem. Soc.*, 2006, **128**, 7476–7485.
39 K. S. Joya, N. K. Subbaiyan, F. D'Souza and H. J. M. Groot, *Angew. Chem., Int. Ed.*, 2012, **51**, 9601–9605.
40 VMD, The molecular representations have been made with the program VMD owned by the Theoretical and Computational Biophysics Group, NIH Resource for Macromolecular Modeling and Bioinformatics, at the Beckman Institute, University of Illinois at Urbana-Champaign: <http://www.ks.uiuc.edu/Research/vmd/>.

